

# Optimal Operation of Multilevel Modular Resonant Switched-Capacitor Converter

Yanchao Li, Ze Ni and Dong Cao  
Electrical and Computer Engineering  
North Dakota State University  
Fargo, North Dakota, United States  
Yanchao.li@ndsu.edu

**Abstract**— Multilevel modular resonant switched-capacitor converter can achieve either zero-current switching (ZCS) or zero-voltage switching (ZVS) by utilizing different converter control strategies. This paper presents a comprehensive way to compare the root mean square (RMS) value of current flowing through switching devices in both ZCS operation and ZVS operation. The study shows that with appropriate converter parameter design, the ZVS operation allows the RMS value of switch current at most 10% lower than that in ZCS operation. Therefore, the converter operating at ZVS mode has the potential to achieve higher efficiency comparing to the converter that operates at ZCS mode due to less semiconductor conduction loss. Furthermore, the ZVS operation can reduce the power loss due to MOSFET output capacitance. A 6x converter with 54V input voltage, 9V output voltage and 600W power rating is used as an example to show the detailed design procedure. Simulation results are provided to verify the theoretical analysis. Also, a 600W lab prototype that has 6 to 1 voltage conversion ratio has been built to verify the theoretical analysis.

**Keywords**— *multilevel, switched-capacitor, comparison, dc-dc converter, phase-shift control, resonant converter, ZCS, ZVS*

## I. INTRODUCTION

The traditional inductor-based switched-mode power supplies (SMPS) have been widely used in different kinds of applications for a long time. For instance, boost converter is used in electric vehicle (EV) applications as an interface between the car battery and the DC-link [1]–[4]. This is because the voltage of the car battery is not high enough to be used by the inverter that drives the motor. Also, boost converter is used in photovoltaic (PV) applications as an interface between PV arrays and DC-link [5]. Nowadays, wide bandgap devices become more and more popular due to their superior reliability and performance [6], [7]. And the size of power converters has been greatly reduced due to the development of wide bandgap devices [8]–[10]. As a result, reducing the size of magnetic components such as inductors becomes the major challenge to achieve high power density and light weight of the inductor-based DC-DC converters. Although the wide bandgap devices help reduce the converter size, it cannot change the fact that the

traditional inductor-based SMPS still needs bulky magnetic components in the circuit. Thus, new converter topologies that require minimum magnetic components are desired.

Switched-capacitor circuits are known as magnetic-less circuits, they only use capacitors as energy transfer media in the circuits. In traditional switched-capacitor circuits, the capacitors in switched-capacitor converters are directly charged or discharged by other capacitors that are connected in series [11], [12]. This kind of switched-capacitor DC-DC power conversion techniques are commonly used in very low power applications. The most representative application area is chip-level application [13]–[19]. For example, the charge pump circuit is one of the most widely used circuits in power management integrated circuits (PMIC). However, when it comes to medium-power or high-power application, the high transient current due to the capacitor charging and discharging during the converter operation will lead to some inevitable issues, such as high power loss and serious electromagnetic interference (EMI) problems [20]. All these issues become fatal drawbacks for the switched-capacitor techniques to be applied to practical industrial applications. In order to reduce the current spike that leads to all kinds of issues, minimizing the voltage ripples on the capacitors is one of the effective approaches [21]. There are two ways to achieve this approach, i.e. increasing switching frequency or using capacitor with high capacitance in the circuit. One major issue of this approach is that the capacitor bank volume cannot be minimized due to the strict voltage ripple requirement. Therefore, the resonant concept is introduced to the switched-capacitor circuits. This kind of converter is called resonant switched-capacitor converter or hybrid switched-capacitor converter.

For the multilevel modular resonant switched-capacitor converter, there are two operation modes, which are ZCS operation mode and ZVS operation mode. Both of the operation modes can achieve very high efficiency [22]–[26]. On one hand, without phase-shift control method, the switching devices in the converter can achieve zero-current switching. On the other hand, with the phase-shift control method, zero-voltage switching of the switching devices can be achieved. This paper analyzes the equivalent circuits of both operation modes and compares the switching device's current waveform. The study shows that the RMS value of the current flowing through switching devices in the ZVS operation can be lower than that in the ZCS operation.

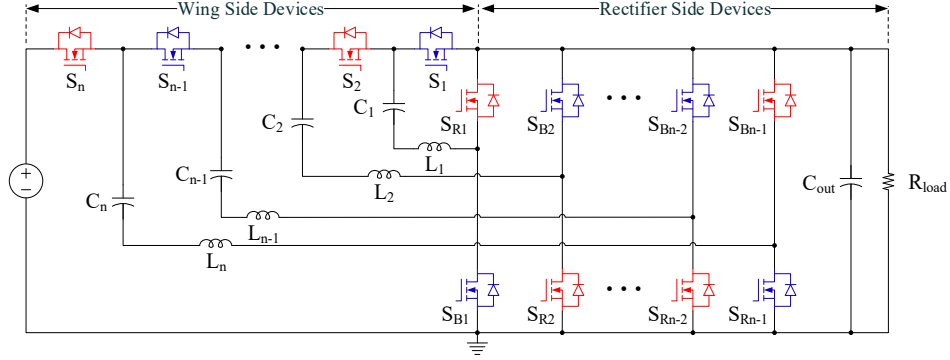


Fig. 1: Circuit configuration of the analyzed converter

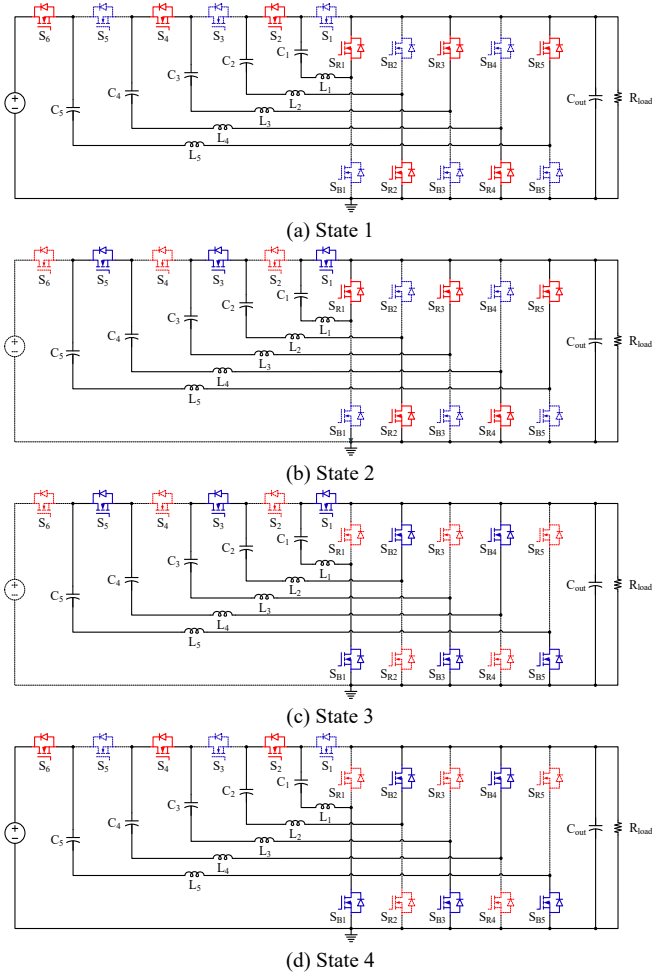


Fig. 2 Equivalent circuits for both ZCS and ZVS operation

But this is only true when the converter is properly designed. Hence, this paper uses an example to show the detailed design procedures that reach the optimum design and ensures the high-performance operation of the presented converter. Simulation and experimental results are provided to validate the theoretical analysis.

## II. CONVERTER CONFIGURATION AND COMPARATIVE STUDY

This section will introduce the circuit configuration of the presented converter at first. Then the zero-voltage switching operation and the zero-current switching operation of the presented converter are demonstrated. A comparative study of the two operation modes is conducted to show that the ZVS operation achieves lower switching device RMS current in the converter, which results in lower semiconductor conduction loss.

### A. Circuit Configuration and Two Operation Modes

Fig. 1 shows the generalized circuit configuration. The switching devices in the presented converter can be classified into two parts. The first part is the rectifier side devices. They constitute the half-bridges that are connected to the ground. The second part is wing side devices. All the wing side devices are floating devices. For a converter with  $N$  times voltage conversion ratio, the number of switching device on the wing side is  $N$ . And the number of switching device on the rectifier side is  $2(N-1)$ . In terms of the wing side devices, the voltage stress of  $S_1$  and  $S_n$  equals to the output voltage, while the voltage stress of switch  $S_2$  to  $S_{n-1}$  is the two times of the output voltage. And the voltage stress of the rectifier side devices is  $V_{out}$ .

The presented converter has two operation modes. And they achieve zero-current switching and zero-voltage switching, respectively. Note that the detailed method of realizing ZCS and ZVS will not be covered in this paper since they have been studied in [23] and [24]. This section focuses on analyzing the switching devices' current waveform for both operation modes and calculating the RMS value of device current. Fig. 2 shows the four equivalent circuits that can be used to analyze the switching devices' current waveform for ZCS and ZVS operations. In order to simplify the analysis, several assumptions have been made:

- All of the switching devices in the analyzed converter are ideal.
- Voltage ripples across all the capacitors in the converter are negligible.

- The effect of the deadtime on the switching device RMS current is negligible.
- The inductance value and capacitance value in all the resonant tanks are identical.

For the ZCS operation, there are only two operation states, which are shown in Fig. 2(a) and Fig. 2(c). In this operation mode, the switching frequency of all switching devices is matched with the resonant frequency of the resonant tank, which can be calculated using (1). Fig. 3 shows the current waveforms of switching devices in ZCS mode. According to Fig. 3, the current flowing through all the switches is sinusoidal waveform.

$$f_s = \frac{1}{T_s} = \frac{1}{2\pi\sqrt{L_r C_r}} \quad (1)$$

For the ZVS operation, the phase-shift control method is used to achieve the soft-switching function. Therefore, there are

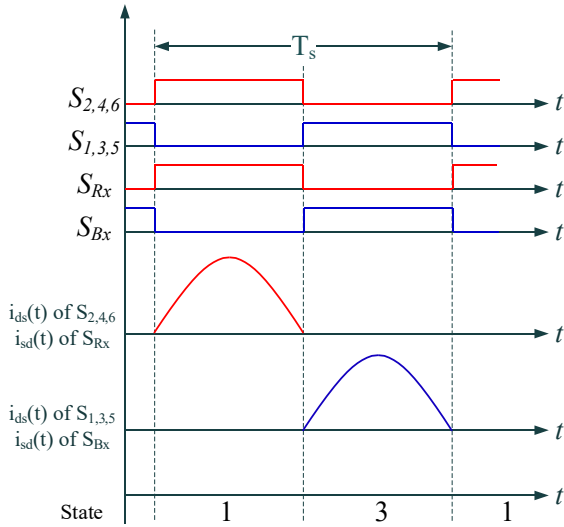


Fig. 3 Switch current waveform when converter operates at ZCS mode

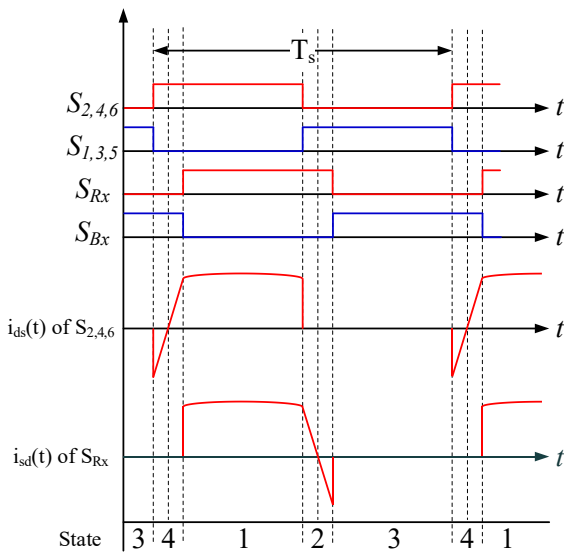


Fig. 4 Switch current waveform when converter operates at ZVS mode

four switching states during the converter operation, whose equivalent circuits are shown as state 1 to state 4 in Fig. 2. The switching frequency for this operation should be higher than the resonant frequency of the resonant tank, as shown in (2). Fig. 4 shows the current waveform of the switching devices in a converter that operates at ZVS mode.

$$f_s > \frac{1}{2\pi\sqrt{L_r C_r}} \quad (2)$$

### B. Target For the Optimized Design

When the presented converter has a certain average output current  $I_{out}$ , the average value of current flowing through each switch can be calculated using (3). In (3), the  $P_{out}$  represents the output power of the converter,  $V_{out}$  represents the output voltage, and  $N$  is the voltage conversion ratio of the converter. It's worth mentioning that this calculation method can be used in both ZCS and ZVS operation modes.

$$I_{sw\_avg} = \frac{I_{out}}{N} = \frac{P_{out}}{V_{out} * N} \quad (3)$$

With the average current information, the amplitude of the switch current in ZCS operation and ZVS operation can be calculated, as shown in (4) and (5). Thus, the switching device RMS current value can also be calculated.

$$I_{sw\_zvs\_peak} = \frac{1}{L_r/V_{out}} * \frac{T_{shift}}{2} \quad (4)$$

$$I_{sw\_zvs\_peak} = \frac{I_{out}\pi}{N} \quad (5)$$

When the converter operates at ZCS operation mode, the switching device RMS current is a function of converter output current. On the other hand, the RMS value of the current flowing through switches depends on converter output current, output voltage, switching frequency and resonant inductance value. Fig. 5 shows the switch current waveform in extreme case while the converter operates at ZVS mode. In the extreme case, the phase-shift time is infinitely close to zero. Although the extreme case is an ideal case, it shows the lowest possible RMS value of switch current in ZVS operation. Fig. 6 shows that the converter with ZVS operation can achieve less semiconductor conduction loss with proper parameter design. And the desired design region of the presented 6x converter is marked in Fig. 6. A design example in the next section will be demonstrated.

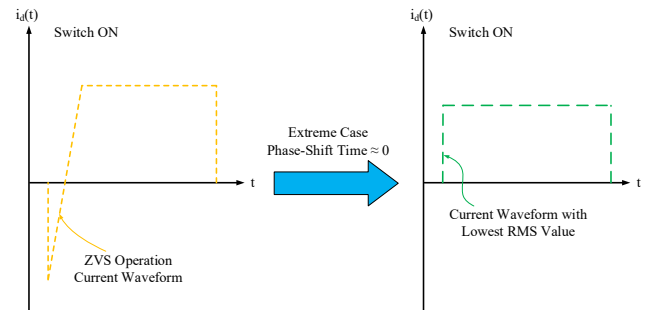


Fig. 5 Switch current waveform in extreme case (ZVS operation)

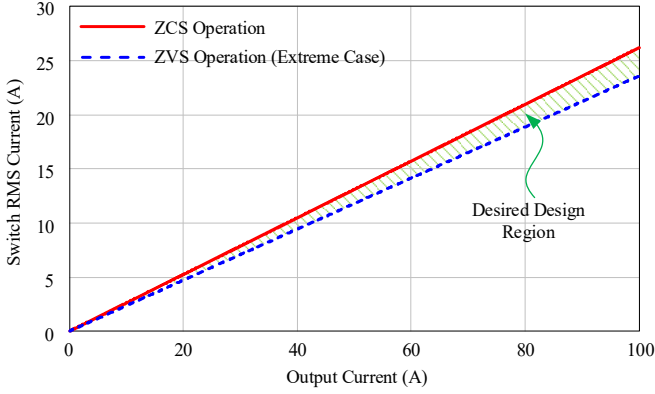


Fig. 6 Target for the optimized design

### III. DESIGN EXAMPLE

In Table I, the basic converter specification used in this design example is provided. The designed converter has 54V input and 9V output. The typical output power is 450W and the maximum output power is 600W. This converter can be used in the data center as an intermediate bus converter. Table II shows the two converters that achieve the same function but with different operation mode, and we assume they use the same switching devices in the converter. In this example, the optimum design of converter #2 allows the converter has less switching device RMS current than converter #1 when they have the same output power. In this design example, because the inductors that have inductance within a hundred nanohenry have been proven to be good choices for this specific design [22], three off-the-shelf inductor candidates are selected as the starting point of this design, as shown in Table III.

TABLE I BASIC CONVERTER SPECIFICATION USED IN THE DESIGN EXAMPLE

Description	Items	Values
Input Voltage	$V_{in}$	54 V
Maximum Input Current	$I_{in}$	11.1V
Output Voltage	$V_{out}$	9 V
Maximum Output Current	$I_{out}$	66.6A
Maximum Output Power	$P_{out\_max}$	600 W
Typical Output Power	$P_{out\_typ}$	450 W
Voltage Conversion Ratio	$N$	6

TABLE II TWO CONVERTERS USED IN THE DESIGN EXAMPLE

Converters	Operation Mode
Converter #1	ZCS Operation
Converter #2	ZVS Operation

TABLE III INDUCTOR CANDIDATES USED IN THE DESIGN EXAMPLE

Part Number	Values
SLC7649S-360KL	36nH
SLC7649S-500KL	50nH
SLC7649S-700KL	70nH

We assume the switching frequency of the converters is 350kHz. According to Fig. 7, when the phase-shift time is 0.25 time of the switching period, the converter #2 can generate the highest output current. Also, with the decrease of resonant inductance, the output current capability of the converter #2 is increased. This means for the same output current, converters with lower inductance have less phase-shift time, and their switching devices' current waveform is closer to the extreme case that mentioned in Fig. 5. Fig. 8 shows the comparison between converter #1 and converter #2 regarding the RMS value of the device current. When resonant inductance is 36nH and the converter outputs the maximum current, the switching devices in converter #1 and converter #2 has the same device RMS current, which means they have the same semiconductor conduction loss. It's worth mentioning that with the increase of output power, the power loss due to device output capacitor can be partially or fully recycled in converter #2, while converter #1 cannot achieve this function. So this design is considered as one of the optimum design points of converter #2, especially the converter for the low voltage high current application.

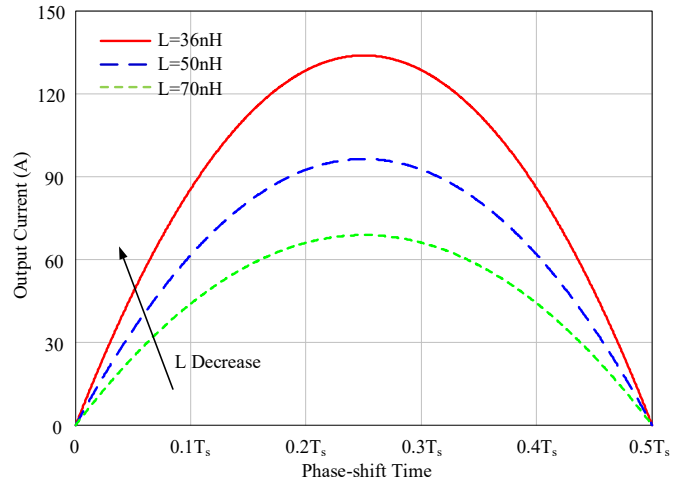


Fig. 7 Output current and phase-shift time relationship ( $f_s=350\text{kHz}$ )

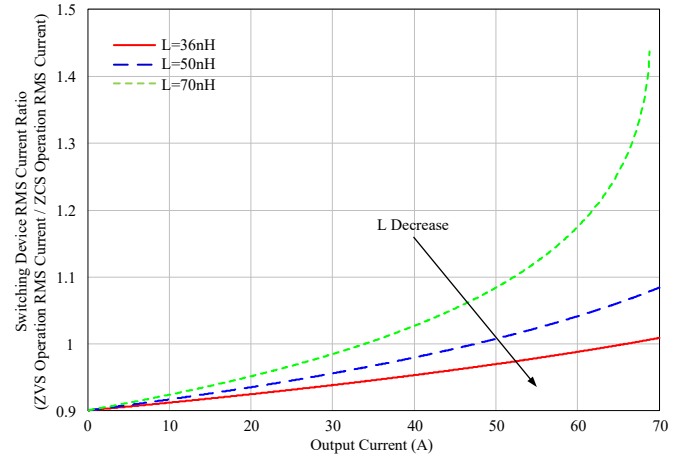


Fig. 8 Output current and device RMS current ratio relationship ( $f_s=350\text{kHz}$ )

#### IV. SIMULATION RESULTS AND EXPERIMENTAL WAVEFORMS

Simulation has been performed to verify the theoretical analysis and show that the switching devices in a converter that operates at ZVS mode have lower RMS current stress than that in the converter operates at ZCS mode. Table IV shows the parameters used to simulate the converter that operates at ZCS mode. Similarly, Table V shows the designed converter parameters for ZVS operation. It is worth mentioning that although converter #1 uses lower capacitance for resonant capacitors, it needs U2J or C0G ceramic capacitors to ensure the accurate resonant operation, whose capacitance density is not as high as the X7R/X5R ceramic capacitors that can be used in converter #2. As a result, the volume of the resonant capacitor bank is very similar in the two converters.

Fig. 9 and Fig. 10 show the switching devices' current waveforms of converter #1 and converter #2, respectively. When the converters have 450W power output, the RMS values of the current flowing through the switches in converter #1 and converter #2 are 13.00A and 12.56A. At this operating point, not only the semiconductor conduction loss is reduced, but also the power loss due to MOSFET output capacitors can be recycled. Fig. 11 shows the inductor waveforms of both converters. Because the inductor ripple current in converter #2 is lower than that in converter #1, the inductor in converter #2 could be more efficient than the inductor in converter #1. Therefore, with the reduced power loss on inductors and semiconductors, the ZVS operation is possible to enable higher efficiency of the presented multilevel modular resonant switched-capacitor converter.

TABLE IV PARAMETERS USED IN THE SIMULATION (CONVERTER #1, ZCS OPERATION)

Items	Symbols	Values
Switching Frequency	$f_s$	354 kHz
Resonant Inductance	$L_r$	36 nH
Resonant Capacitance	$C_r$	5.64 $\mu$ F
Output Power	$P_{out}$	450 W

TABLE V PARAMETERS USED IN THE SIMULATION (CONVERTER #2, ZVS OPERATION)

Items	Symbols	Values
Switching Frequency	$f_s$	350 kHz
Resonant Inductance	$L_r$	36 nH
Resonant Capacitance	$C_r$	120 $\mu$ F
Output Power	$P_{out}$	450 W

A lab prototype that is capable of delivering 600W maximum power has been developed to verify the theoretical analysis and simulation results. The GaN-based prototype uses EPC2023 as switching devices. Because measuring the current waveform of each switching device is difficult, inductor waveforms are measured instead. Fig. 12 shows the inductor waveform when the converter operates at ZVS operation mode. And Fig. 13 shows the inductor current waveform when the presented converter operates at ZCS operation mode. And the

RMS value of the former current waveform is lower than the later one, which matches with the theoretical analysis.

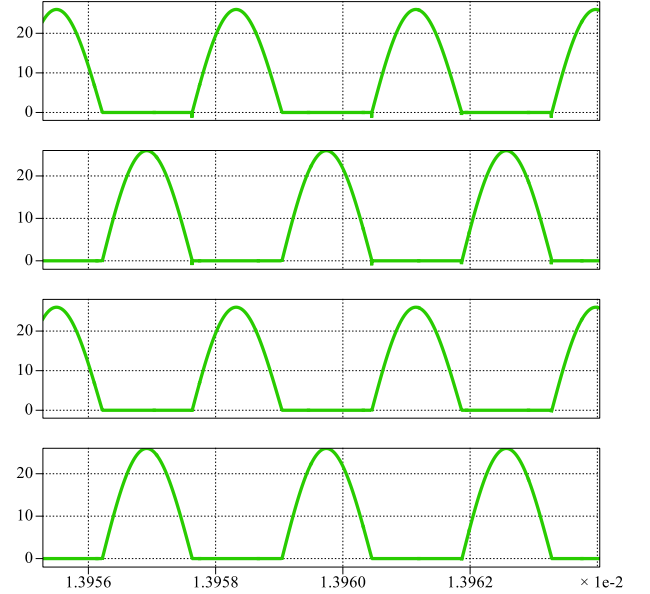


Fig. 9 Switch current waveforms when converter operates at ZCS mode

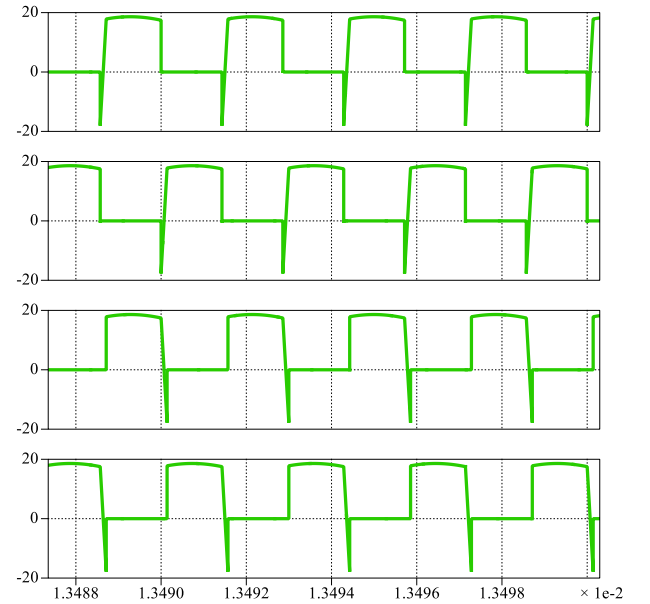


Fig. 10 Switch current waveforms when converter operates at ZVS mode

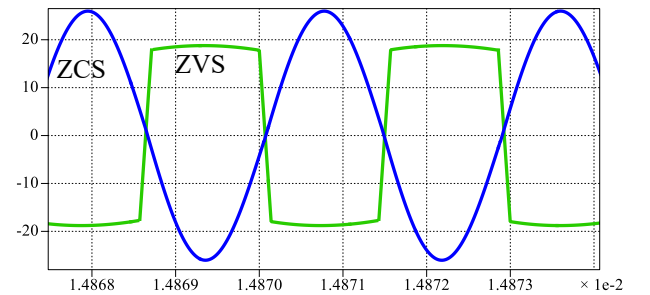


Fig. 11 Inductor current waveform comparison

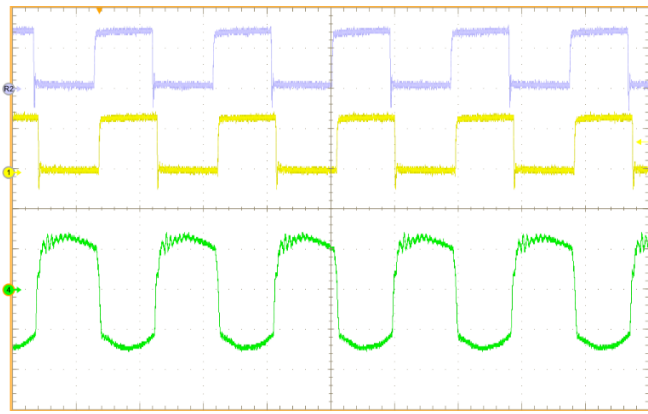


Fig. 12 Inductor current waveform when converter operates at ZVS mode

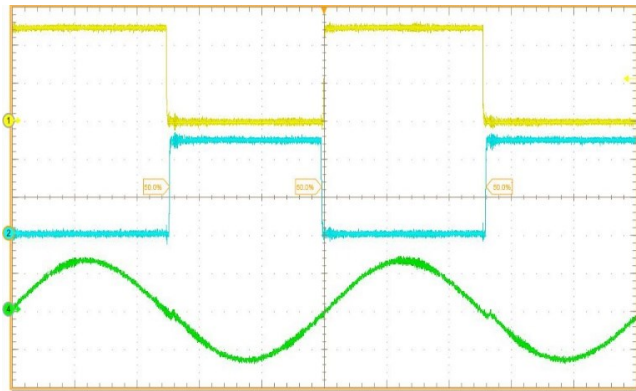


Fig. 13 Inductor current waveform when converter operates at ZCS mode

## V. CONCLUSION

This paper compares two soft-switching mechanisms of the presented 6x multilevel modular resonant switched-capacitor converter. The study shows that compared with ZCS operation mode, ZVS operation mode of the converter can reduce the power loss of semiconductors and inductors. A design example has been performed to show the design procedure of the presented converter. Simulation results and experimental waveforms are provided in the paper to verify the theoretical analysis.

## ACKNOWLEDGMENT

The authors would like to thank Efficient Power Conversion Corporation for its engineering samples and support.

## REFERENCES

[1] X. Jia, D. Xu, S. Du, C. Hu, M. Chen, and P. Lin, "A High Power Density and Efficiency Bi-Directional DC / DC Converter for Electric Vehicles," *Proc. Int. Conf. Power Electron. ECCE Asia, Seoul*, pp. 874–880, 2015.

[2] L. Chen, "A variable voltage converter with direct bypass for traction drive inverters," in *2013 IEEE Energy Conversion Congress and Exposition*, 2013, pp. 2793–2798.

[3] Serkan Öztürk, "Design of three phase interleaved DC/DC boost converter with all SiC semiconductors for electric vehicle applications," *2017 10th Int. Conf. Electr. Electron. Eng.*, 2017.

[4] A. Emadi, S. S. Williamson, and A. Khaligh, "Power electronics

intensive solutions for advanced electric, hybrid electric, and fuel cell vehicular power systems," *IEEE Trans. Power Electron.*, vol. 21, no. 3, pp. 567–577, May 2006.

[5] W. Li and X. He, "Review of Nonisolated High-Step-Up DC/DC Converters in Photovoltaic Grid-Connected Applications," *IEEE Trans. Ind. Electron.*, vol. 58, no. 4, pp. 1239–1250, Apr. 2011.

[6] Z. Ni, Y. Li, X. Lyu, O. P. Yadav, and D. Cao, "Miller plateau as an indicator of SiC MOSFET gate oxide degradation," in *Conference Proceedings - IEEE Applied Power Electronics Conference and Exposition - APEC*, 2018, vol. 2018–March, pp. 1280–1287.

[7] Z. Ni, X. Lyu, O. P. Yadav, and D. Cao, "Review of SiC MOSFET based three-phase inverter lifetime prediction," in *Conference Proceedings - IEEE Applied Power Electronics Conference and Exposition - APEC*, 2017, pp. 1007–1014.

[8] X. Lyu, N. Ren, Y. Li, and D. Cao, "A SiC-Based High Power Density Single-Phase Inverter With In-Series and In-Parallel Power Decoupling Method," *IEEE J. Emerg. Sel. Top. Power Electron.*, vol. 4, no. 3, pp. 893–901, Sep. 2016.

[9] H. Kim *et al.*, "SiC-MOSFET composite boost converter with 22 kW/L power density for electric vehicle application," in *2017 IEEE Applied Power Electronics Conference and Exposition (APEC)*, 2017, pp. 134–141.

[10] X. Lyu, Y. Li, and D. Cao, "DC-Link RMS Current Reduction by Increasing Paralleled Three-Phase Inverter Module Number for Segmented Traction Drive," *IEEE J. Emerg. Sel. Top. Power Electron.*, vol. 5, no. 1, pp. 171–181, Mar. 2017.

[11] F. Zhang, L. Du, F. Z. Peng, and Z. Qian, "A new design method for high-power high-efficiency switched-capacitor DC-DC converters," *IEEE Trans. Power Electron.*, vol. 23, no. 2, pp. 832–840, Mar. 2008.

[12] D. Gunasekaran, L. Qin, U. Karki, Y. Li, and F. Z. Peng, "A Variable (n/m)X Switched Capacitor DC–DC Converter," *IEEE Trans. Power Electron.*, vol. 32, no. 8, pp. 6219–6235, Aug. 2017.

[13] C. Schaefer, K. Kesarwani, and J. T. Stauth, "20.2 A variable-conversion-ratio 3-phase resonant switched capacitor converter with 85% efficiency at 0.91W/mm<sup>2</sup> using 1.1nH PCB-trace inductors," in *2015 IEEE International Solid-State Circuits Conference - (ISSCC) Digest of Technical Papers*, 2015, pp. 1–3.

[14] K. Kesarwani, R. Sangwan, and J. T. Stauth, "A 2-phase resonant switched-capacitor converter delivering 4.3W at 0.6W/mm<sup>2</sup> with 85% efficiency," *Dig. Tech. Pap. - IEEE Int. Solid-State Circuits Conf.*, vol. 57, pp. 86–87, Feb. 2014.

[15] C. Schaefer and J. T. Stauth, "A 3-Phase Resonant Switched Capacitor Converter Delivering 7.7 W at 85% Efficiency Using 1.1 nH PCB Trace Inductors," *IEEE J. Solid-State Circuits*, vol. 50, no. 12, pp. 2861–2869, 2015.

[16] H. P. Le, M. Seeman, S. R. Sanders, V. Sathe, S. Naffziger, and E. Alon, "A 32nm fully integrated reconfigurable switched-capacitor DC-DC converter delivering 0.55W/mm<sup>2</sup> at 81% efficiency," in *Digest of Technical Papers - IEEE International Solid-State Circuits Conference*, 2010, vol. 53, pp. 210–211.

[17] Y. Lee *et al.*, "Raven: A 28nm RISC-V vector processor with integrated switched-capacitor DC-DC converters and adaptive clocking," in *2015 IEEE Hot Chips 27 Symposium, HCS 2015*, 2016, pp. 1–45.

[18] K. Kesarwani, R. Sangwan, and J. T. Stauth, "Resonant switched-capacitor converters for chip-scale power delivery: Modeling and design," in *2013 IEEE 14th Workshop on Control and Modeling for Power Electronics, COMPEL 2013*, 2013, pp. 1–7.

[19] K. Kesarwani, R. Sangwan, and J. T. Stauth, "Resonant-Switched Capacitor Converters for Chip-Scale Power Delivery: Design and Implementation," *IEEE Trans. Power Electron.*, vol. 30, no. 12, pp. 6966–6977, 2015.

[20] Y. Lei, R. May, and R. Pilawa-Podgurski, "Split-Phase Control: Achieving Complete Soft-Charging Operation of a Dickson Switched-Capacitor Converter," *IEEE Trans. Power Electron.*, vol. 31, no. 1, pp. 770–782, 2016.

[21] G. Y. Zhu and A. Ioinovici, "Steady-state characteristics of

switched-capacitor electronic converters,” *J. Circuits, Syst. Comput.*, vol. 7, no. 02, pp. 69–91, 1997.

- [22] Y. Li, X. Lyu, D. Cao, S. Jiang, and C. Nan, “A 98.55% Efficiency Switched-Tank Converter for Data Center Application,” *IEEE Trans. Ind. Appl.*, pp. 1–1, 2018.
- [23] Y. Li, X. Lyu, D. Cao, S. Jiang, and C. Nan, “A high efficiency resonant switched-Capacitor converter for data center,” in *2017 IEEE Energy Conversion Congress and Exposition, ECCE 2017*, 2017, vol. 2017–Janua, pp. 4460–4466.
- [24] Y. Li, B. Curuvija, X. Lyu, and D. Cao, “Multilevel modular switched-capacitor resonant converter with voltage regulation,” in *2017 IEEE Applied Power Electronics Conference and Exposition (APEC)*, 2017, pp. 88–93.
- [25] M. Shoyama, F. Deriha, and T. Ninomiya, “Resonant boost switched capacitor converter with high efficiency,” in *30th Annual Conference of IEEE Industrial Electronics Society, 2004. IECON 2004*, vol. 1, pp. 222–226.
- [26] K. Sano and H. Fujita, “Performance of a high-efficiency switched-capacitor-based resonant converter with phase-shift control,” *IEEE Trans. Power Electron.*, vol. 26, no. 2, pp. 344–354, 2011.